Electric field distribution around the chain of composite nanoparticles in ferrofluids*

Fan Chun-Zhen(范春珍)[a)b)†], Wang Jun-Qiao(王俊俏)[a)], Cheng Yong-Guang(程永光)[a)], Ding Pei(丁 佩)[c)], Liang Er-Jun(梁二军)[a)‡], and Huang Ji-Ping(黄吉平)[b)§]

[a)] School of Physical Science and Engineering, and Key Laboratory of Materials Physics of Ministry of Education of China, Zhengzhou University, Zhengzhou 450052, China

[b)] State Key Laboratory of Surface Physics and Department of Physics, Fudan University, Shanghai 200433, China

[c)] Department of Mathematics and Physics, Zhengzhou Institute of Aeronautical Industry Management, Zhengzhou 450015, China

(Received 25 December 2012; revised manuscript received 15 April 2013)

Composite nanoparticles (NPs) have the ability of combining materials with different properties together, thus receiving extensive attention in many fields. Here we theoretically investigate the electric field distribution around core/shell NPs (a type of composite NPs) in ferrofluids under the influence of an external magnetic field. The NPs are made of cobalt (ferromagnetic) coated with gold (metallic). Under the influence of the external magnetic field, these NPs will align along the direction of this field, thus forming a chain of NPs. According to Laplace's equations, we obtain electric fields inside and outside the NPs as a function of the incident wavelength by taking into account the mutual interaction between the polarized NPs. Our calculation results show that the electric field distribution is closely related to the resonant incident wavelength, the metallic shell thickness, and the inter-particle distance. These analytical calculations agree well with our numerical simulation results. This kind of field-induced anisotropic soft-matter systems offers the possibility of obtaining an enhanced Raman scattering substrate due to enhanced electric fields.

Keywords: core/shell nanoparticles, electric field distribution, Laplace's equation

PACS: 47.65.Cb, 41.20.Cv **DOI:** 10.1088/1674-1056/22/8/084703

1. Introduction

The core/shell nanoparticle (NP) is a kind of composite, having the ability of combining materials with different properties together. It has become a burgeoning research area in recent years,[1] not only due to its capability to include its own intrinsic properties, but also because it can result in some unique properties arising from the coupling of coating and interior components, which is beyond the intrinsic limitation of individual components.[2] One of the most intensively studied core/shell nanocomposites is the ferromagnetic NP coated with a metallic shell,[3] incorporating optically active components onto magnetic cores.[4] For these nanoscale composites, their unique physical and chemical properties are contributed from the altered high surface area to volume ratio and modified surface functionalization.[5] With magnetic cores, the magnetic NPs will have a response to the applied magnetic field, and the metallic coating also renders the magnetic NPs with plasmonic properties[4] and enhanced bio-compatibility. This makes the core/shell NPs presently active composites in the applications of bio-separation, catalysts, contrast agents for magnetic resonance imaging, and so on. Up to now, a lot of researches, either theoretical or experimental, have been carried out to synthesize and characterize the ferromagnetic core/shell structures, typically including iron oxide metallic shell,[6] Fe_3O_4@Au,[7] Fe_3O_4@Ag,[8] etc.[9–13] To fabricate core/shell magnetic nanocomposites, magnetic NPs can be obtained with wet chemical processes in aqueous systems and the metallic shell can be reduced at the NP surface to add a metal layer, which can then be functionalized with thiolated molecules via a covalent bond to the surface of the NPs.[14,15]

The ferromagnetic nanocomposites will form an ordered chain with the applied magnetic field. Enhanced electromagnetic field effects can be generated close to the metal surface, which stem from the electromagnetic coupling between nanoparticles or from periodically ordered metal nanostructures, making it possible to transfer optical signals along the nanoparticle array.[16–20] In this paper, we emphasize on the mutual interaction between core/shell NPs in ferrofluids under the influence of the external magnetic field. The ferrofluid is a type of colloidal suspension, in which single domain magnetic

*Project supported by the National Natural Science Foundation of China (Grant Nos. 11104252 and 11222544), the Science Fund of the Ministry of Education of China (Grant No. 20114101110003), the Fund for Science and Technology Innovation Team of Zhengzhou City (2011-03), the Aeronautical Science Foundation of China (Grant No. 2011ZF55015), the Basic and Frontier Technology Research Program of Henan Province, China (Grant Nos. 112300410264 and 122300410162), the Cooperation Fund with Fudan University, China (Grant No. KL2011-01), the Fok Ying Tung Education Foundation, China (Grant No. 131008), the Program for New Century Excellent Talents in University (Grant No. NCET-12-0121), and the National Key Basic Research Program of China (Grant No. 2011CB922004).

†Corresponding author. E-mail: chunzhen@zzu.edu.cn

‡Corresponding author. E-mail: ejliang@zzu.edu.cn

§Corresponding author. E-mail: jphuang@fudan.edu.cn

© 2013 Chinese Physical Society and IOP Publishing Ltd

particles (about 10 nm in diameter) are dispersed in the polar or non-polar liquid.[21,22] The ferromagnetic NPs are taken as cobalt coated by gold (Co@Au) in the host fluid (water). With the solution of the Laplace's equations, the electric field distributions inside and outside the NPs are obtained as a function of the incident wavelength. Namely, analytical expressions are derived for the electric field distributions around the ferromagnetic nanocomposites as a function of the radial distance. As we know, it is often required that electromagnetic materials have specified values of the electric field or magnetic permeability in engineering applications. With the aid of analytical expressions, a composite material prepared by dispersing uniformly a fine metal powder in a homogeneous dielectric matrix has an effective dielectric constant that can be controlled by varying the powder loading volume.[23] Specifically, magnetic nanoparticles with an encapsuled thin oxide layer (around 5 nm) can avoid the degradation of the magnetic properties by oxidation and moreover reduce the eddy current loss.[3] Resorting to these analytical expressions, our numerical results show that the maximum magnitude of the electric filed is closely related to the resonant incident wavelength, the metallic shell thickness, and the inter-particle distance. These analytical results are validated by the simulation results.

2. Formulism

Now, let us turn to the issue of the electric field distribution around the core/shell NPs in the ferromagnetic NPs chain. The spherical nanocomposites with radius R and effective dielectric constant $\varepsilon_{\rm e}(\omega)$ are suspending in the host liquid. Under the applied field, the Maxwell equations can be written as

$$\nabla \cdot \boldsymbol{D} = 0, \tag{1}$$

$$\nabla \times \boldsymbol{E} = 0. \tag{2}$$

In the spherical coordinates (r,θ,φ), the electric potentials inside and outside the nanocomposites can be expressed as

$$\Phi_{\rm in}(r,\theta,\varphi) = \sum_{n=0}^{\infty}\sum_{m=0}^{n} A_{nm}\left(\frac{r}{R}\right)^n \mathrm{Y}_{nm}(\theta,\varphi), \quad r<R \tag{3}$$

and

$$\Phi_{\rm out}(r,\theta,\varphi) = \sum_{n=0}^{\infty}\sum_{m=0}^{n}\left[B_{nm}\left(\frac{r}{R}\right)^n + C_{nm}\left(\frac{R}{r}\right)^{n+1}\right]\mathrm{Y}_{nm}(\theta,\varphi), \quad r>R \tag{4}$$

respectively, where $\mathrm{Y}_{nm} = \mathrm{P}_n(\cos\theta)\cos m\varphi$ and $\mathrm{P}_n(\cos\theta)$ is the associated Legendre polynomial function. The summation of n runs over all NPs except the one at the origin. A_{nm}, B_{nm}, and C_{nm} are the Laplacian coefficients, which can be determined by boundary conditions

$$\Phi_{\rm in}(r,\theta,\varphi)|_{r=R} = \Phi_{\rm out}(r,\theta,\varphi)|_{r=R}, \tag{5}$$

$$\varepsilon_{\rm e}(r)\frac{\partial\Phi_{\rm in}(r,\theta,\varphi)}{\partial r}\bigg|_{r=R} = \varepsilon_m\frac{\partial\Phi_{\rm out}(r,\theta,\varphi)}{\partial r}\bigg|_{r=R}. \tag{6}$$

Solving the above equations, we obtain

$$B_{nm} = \frac{(1+K)n+1}{(1-K)n}C_{nm} = D_nC_{nm}, \tag{7}$$

$$A_{nm} = \frac{2n+1}{(1-K)n}C_{nm} = F_nC_{nm}. \tag{8}$$

Thus,

$$D_n = \frac{(1+K)n+1}{(1-K)n}, \tag{9}$$

$$F_n = \frac{2n+1}{(1-K)n}, \tag{10}$$

where K represents the ratio of the effective dielectric constant of NPs to that of the host medium, namely $K = \varepsilon_{\rm e}/\varepsilon_m$. The terms in Eq. (4) with negative powers of r are the multiple potential induced on itself. But the terms with positive powers of r come from the applied field and the multiple moments on all the other NPs. To fully get the expression of these coefficients, one more relation is needed to determine the coefficient C_{nm}. It can be found by equating the field about a central sphere in positive powers of r with the field about the neighboring spheres in negative powers of ρ_i as shown in Fig. 1, where ρ_i,θ_i, and φ_i are the spherical polar coordinates of the point r in a coordinate system with the origin at the center of the i-th sphere. It leads to the following identity,[23,24]

$$\sum_{n,m} B_{nm}\left(\frac{r}{R}\right)^n \mathrm{Y}_{nm}(\theta,\varphi) = \sum_i\sum_{n,m} C_{nm}\left(\frac{R}{\rho_i}\right)^{n+1}\mathrm{Y}_{nm}(\theta_i,\varphi_i) + E_0 r\cos(\theta), \tag{11}$$

where $(\rho_i,\theta_i,\varphi_i)$ are the coordinates relative to the i-th spherical nanoparticle. A series of equations in $C_{n,m}$ may be obtained from Eq. (11). This procedure was first performed by Lam[23] and later employed by Miller and Jones.[24] Thus, by multiplying Eq. (11) by $\mathrm{Y}_{n,m}(\theta,\varphi)$ and integrating over the whole volume, we have

$$E_0R\delta_{2n-1,1} = D_{2n-1}C_{2n-1} + 2\sum_{n'=1}^{\infty}\frac{(2n+2n'-2)!}{(2n-1)!(2n'-1)!}\left(\frac{R}{L}\right)^{(2n+2n'-1)} \times C_{2n'-1}SUM(n+n'), \tag{12}$$

where

$$Q_{2n-1,2n'-1} = \frac{2(2n+2n'-2)!}{(2n-1)!(2n'-1)!}SUM(n+n') \tag{13}$$

and

$$SUM(n+n') = \sum_{i=1}^{\infty}\mathrm{i}^{-(2n-1)}. \tag{14}$$

We define $\lambda = R/L$, where L is the inter distance between two NPs.

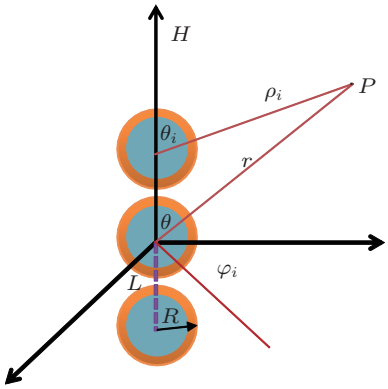


Fig. 1. (color online) Schematic view of a chain of core/shell NPs under the influence of an external magnetic field.

Finally, we replace n and n' with $2n-1$ and $2n'-1$, and equation (12) becomes,

$$\frac{C_{2n-1}}{C_1} = \frac{E_0 A \delta_{2n-1,1}}{D_{2n-1}C_1} - \frac{1}{D_{2n-1}} Q_{2n-1,1}\lambda^{2n+1} - \frac{1}{D_{2n-1}} \times \sum_{n'=2}^{\infty} \lambda^{2n+2n'-1} Q_{2n-1,2n'-1} \frac{C_{2n'-1}}{C_1}. \quad (15)$$

Now, the relations of the three coefficients A_{nm}, B_{nm}, and C_{nm} have already been obtained. By solving the above equations, the potentials inside and outside the NPs are

$$\begin{aligned} \phi_{\text{ind}}(r,\theta) &= \sum_{n=1}^{\infty} G_{2n-1}C_{2n-1}\left(\frac{r}{R}\right)^{2n-1} \times \mathrm{P}_{2n-1}(\cos(\theta)), \quad r<R, \\ \phi_{\text{out}}(r,\theta) &= \sum_{n=1}^{\infty}\left(D_{2n-1}C_{2n-1}\left(\frac{r}{R}\right)^{2n-1} + C_{2n-1}\left(\frac{R}{r}\right)^{2n}\right) \times \mathrm{P}_{2n-1}(\cos(\theta)), \quad r>R. \end{aligned} \quad (16)$$

Thus, the induced electric fields inside and outside core/shell NPs can be obtained through the derivative of the potential[25]

$$E_r = -\frac{\partial\phi}{\partial r}, \qquad E_\theta = -\frac{\partial\phi}{r\partial\theta}. \quad (17)$$

Finally, the electric field around the NPs can be expressed as

$$\begin{aligned} E_r(\text{ind}) &= -\frac{1}{R}\sum_{n=1}^{\infty}(2n-1)G_{2n-1}C_{2n-1}\left(\frac{r}{R}\right)^{2n-2}P_{2n-1}, \\ E_\theta(\text{ind}) &= -\frac{1}{R}\sum_{n=1}^{\infty}G_{2n-1}C_{2n-1}\left(\frac{r}{R}\right)^{2n-2}P'_{2n-1}, \\ E_r(\text{out}) &= -\frac{1}{R}\sum_{n=1}^{\infty}\left((2n-1)D_{2n-1}\left(\frac{r}{R}\right)^{2n-2} - 2n\left(\frac{R}{r}\right)^{2n+1}\right)C_{2n-1}P_{2n-1}, \\ E_\theta(\text{out}) &= -\frac{1}{R}\sum_{n=1}^{\infty}\left(D_{2n-1}\left(\frac{r}{R}\right)^{2n-2} + 2n\left(\frac{R}{r}\right)^{2n+1}\right)C_{2n-1}P'_{2n-1}. \end{aligned} \quad (18)$$

In our numerical calculations, cobalt ferromagnetic NPs coated with gold (Co@Au) are investigated under the influence of the external magnetic field. The schematic structure of the core/shell NPs is illustrated in Fig. 1, where the core/shell NPs align a chain along the external magnetic field direction (H). For most metals at room temperature, the dielectric constant is a function of the incident light frequency, which is expressed in a complex form.[26] To get the effective dielectric constant of the core/shell composites, the dielectric constant of Au shell is chosen as $\varepsilon_1(\omega)$ following a Drude critical points model,[27] which is valid for noble metals within the frequency range of interest and has a perfect match with the experiment data obtained by John and Christy in 1972.[28] The dielectric constant of Co core ferromagnetic NPs (ε_2) was set as $-25+4\mathrm{i}$.[29] Thus, the equivalent linear dielectric constant $\varepsilon_{\text{e}}(\omega)$ for the core/shell composite NPs can be obtained by the Maxwell–Garnett formula,[30,31] which describes a two-component composite where many particles with the dielectric constant ε_{e} and volume fraction f are randomly embedded in a host medium. Thus,

$$\frac{\varepsilon_{\text{e}}(\omega)-\varepsilon_2(\omega)}{\varepsilon_{\text{e}}(\omega)+2\varepsilon_2(\omega)} = f\frac{\varepsilon_1(\omega)-\varepsilon_2(\omega)}{\varepsilon_1(\omega)+2\varepsilon_2(\omega)}, \quad (19)$$

where f is the volume ratio of the magnetic core to the whole coated NPs. The Maxwell–Garnett formula follows from a well-known asymmetrical effective medium theory, and may thus be valid for a low concentration of NPs in the composites.[32] The host liquid is water with the dielectric constant $\varepsilon_m = 1.77$.

Numerical electromagnetic simulations are carried out with the commercial software Comsol Multiphysics to check the local electric field distribution. Transverse magnetic (TM) wave propagation in the plane is considered through the harmonic propagation analysis. Periodic boundary conditions are used for the ferromagnetic particles along the chain direction. Perfectly matched layers are also applied in the propagation direction to eliminate nonphysical reflections at domain boundaries. In our simulation, the core/shell nanocomposites are chosen as Co@Au, and the dielectric constants of the cobalt and gold are taken as the same parameter in the numerical calculation. Radius of the core/shell NPs is fixed as $R = 10$ nm, which is feasible to realize in the experiment.[33] The inner radii are chosen as 5 nm, 6 nm, 7 nm, and 8 nm, respectively. We express the thickness of the core/shell NPs as 5/5, 6/4, 7/3, and 8/2 for simplicity.

3. Results and discussions

Local electric fields around the core/shell ferromagnetic NPs are considered with the influence of the external magnetic field. Based on the solution of Eq. (18), the calculated results

of the electric field distribution outside the NPs E_{out} as a function of the volume fraction f of the core/shell NPs in the suspension are shown in Fig. 2, where the incident wavelength λ is from 100 nm to 1000 nm. Here the inter-particle distance L is taken as 2.2 times the radius of the nanocomposite, namely, $L = 2R$. Numerical results show that two resonant peaks can be obviously observed when the volume fraction f is smaller than 0.3. The resonant peak in the high frequency region tends to disappear with larger f and the magnitude of the resonant peak in the low frequency region is becoming weaker. A smaller f represents a thicker shell layer. Thus, these resonant peaks are arising from the interaction of the free electrons inside the metallic Au layer with a small f. Specifically, when f equals 1.0, there is no resonant peak at all. The whole system is now becoming one suspension where only the cobalt ferromagnetic NPs are distributed in the water. Therefore, the electric field around NPs comes to appear based on the mutual interaction among the polarized core/shell NPs. To verify these results, we have done the simulation by increasing the shell thickness from 2 nm, 3 nm, and 4 nm to 5 nm with the overall radius of the core/shell NPs being 10 nm. The results are given in Fig. 3. The expression of 6/4 means that the radius of the core is 6 nm and that of the shell thickness is 4 nm. The same do the expressions of 5/5, 7/3, and 8/2 mean. As shown in Fig. 3, two resonant peaks can also be found and when the shell thickness decreases from 5 nm to 2 nm, the resonant peak in the high frequency region is becoming smaller. The good match between the analytical and the simulation results indicates that our research on the electric field distribution in ferrofluids is correct.

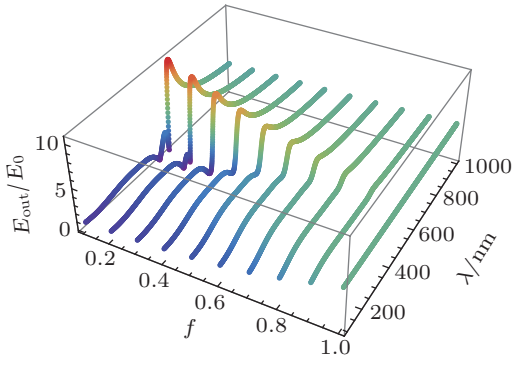


Fig. 2. (color online) Analytical results of the electric field distribution (E_{out}) as a function of the volume fraction f with the incident wavelength λ from 100 nm to 1000 nm. Parameters: $L = 2.2\,R$ and $\theta = \pi/4$.

In Fig. 4, the electric field distribution around the core/shell NPs as a function of the inter-particle distance L with the incident wavelength λ from 100 nm to 1000 nm was investigated. In this case, the volume fraction of the NPs is fixed to $f = 0.3$. As shown in Fig. 4, the strong mutual interaction occurs when L is 2.01 nm, originating predominantly from the coupling of free electrons in the metallic layer. With a gradual increase of L, the magnitudes of resonant peaks are getting weaker, and the resonant peak in the higher frequency region tends to disappear. The simulation results are shown in Fig. 5. The solid, dashed, and dotted lines represent L being 2.2 nm, 2.3 nm, and 2.4 nm, respectively. The resonant peak in the higher frequency region does not exist in the dotted line, which indicates that the strong interaction of free electrons occurs when two core/shell NPs are very close to each other. Numerical calculation matches well with the simulation by comparing Fig. 4 and Fig. 5. Thus, the inter-particle distance has a close relation with the interaction of free electrons in the metallic layer and these resonant peaks arise from the mutual interaction from neighboring particles.

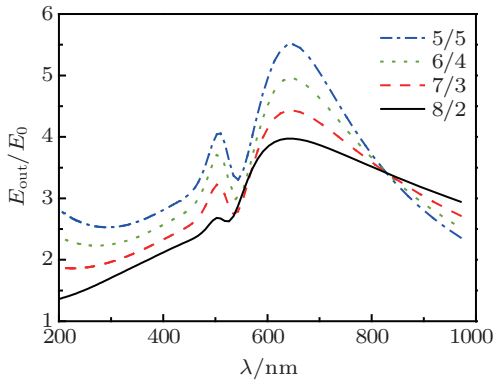


Fig. 3. (color online) Simulation results of the electric filed distribution (E_{out}) with different shell thickness. The radius of the NPs, R, is fixed as 10 nm. The solid, dash, dot, dash–dot lines represent the shell thickness being 5 nm, 4 nm, 3 nm, and 2 nm, respectively. Parameters: L = 2.2 R and $\theta = \pi/4$.

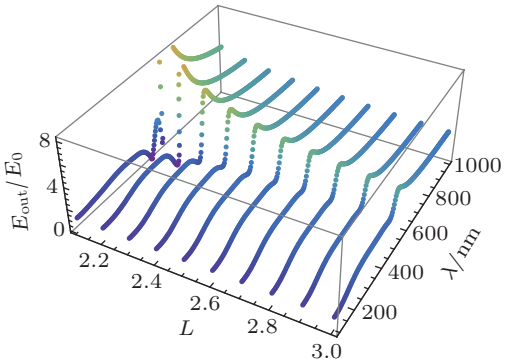


Fig. 4. (color online) Analytical results of electric field distribution (E_{out}) as a function of the inter-particle distance parameter L with the incident wavelength λ from 100 nm to 1000 nm. Parameters: $f = 0.3$ and $\theta = \pi/4$.

All the above results on the electric field distribution are performed with a fixed angle point $\theta = \pi/4$. Now, we are in a position to consider the distribution of electric field around core/shell NPs when θ is ranging from 0° to 90°. The results are illustrated in Fig. 6 with the solution of Eq. (18). It is clearly observed that the electric field decreases gradually when θ is approaching 90 degrees. Moreover, the magnitude of E_{out} can effectively be tuned through the variation of the volume fraction of the shell layer. When f is taken from 0.3

and 0.4 to 0.5, Figure 6(a) shows an overall decrease in the magnitude of E_{out}. This tendency is verified by our simulation results in Fig. 6(b) through varying the shell thickness from 4 nm and 3 nm to 2 nm.

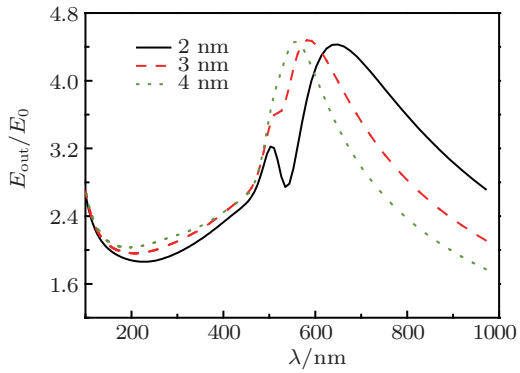


Fig. 5. (color online) Simulation results of electric field distribution (E_{out}) with different inter-particle distance L. The shell thickness is fixed as 3 nm. The solid, dash, dot lines represent inter distance $L = 2.2$ R, 2.3 R, and 2.4 R, respectively. Parameter: $\theta = \pi/4$.

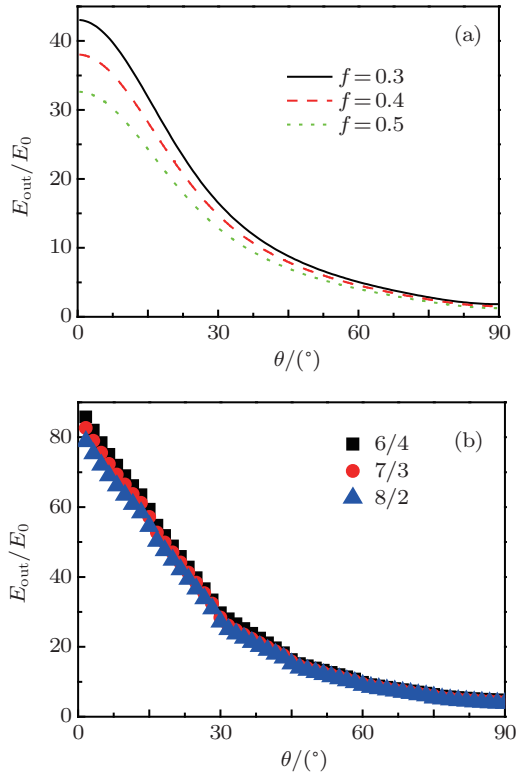


Fig. 6. (color online) (a) Analytical results of electric field distribution (E_{out}) around the NPs surface are illustrated by varying the radial angle θ from 0° to 90°. Parameters: $L = 2.2R$, $f = 0.3$, and $\lambda = 580$ nm. (b) Simulation results of electric field distribution (E_{out}) around the NPs surface are shown with the radial angle θ from 0° to 90°. Parameters: $L = 2.2R$, $r = 7/3$, and $\lambda = 580$ nm.

Finally, we turn to the issue of the magnitude of the electric field distribution inside and outside the NPs. Analytical results are shown in Fig. 7(a) and Fig. 7(b). The distribution tendency is similar, but the magnitude of the one outside is almost nine times larger than that of the one inside. Such large enhancement of the electric filed around core/shell NPs will offer the possibility of obtaining the hot spot, which is the key factor to get an enhanced Raman scattering substrate.

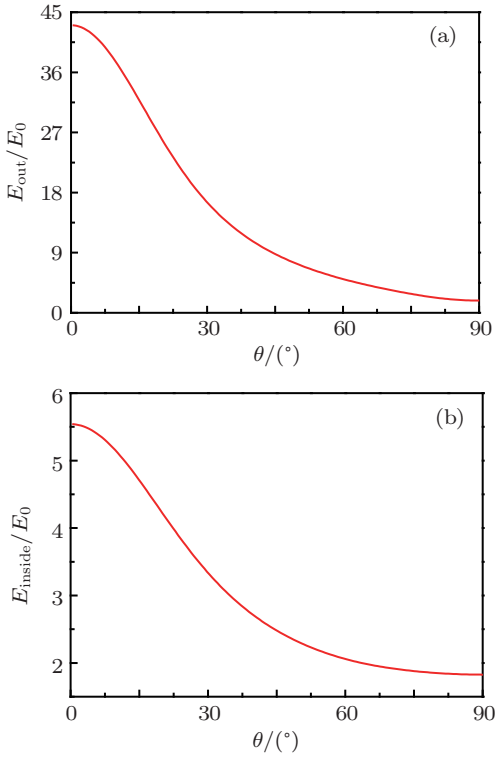


Fig. 7. (color online) Analytical results of electric field distribution (E_{out} and E_{inside}) around the NPs surface by varying the radial angle θ from 0° to 90°. Parameters: $L = 2.2R$, $f = 0.3$, and $\lambda = 580$ nm.

4. Conclusions

In conclusion, we have studied the electric field distribution around the core/shell ferromagnetic NPs in ferrofluids with the solution of Laplace's equations. Resonant peaks of the local electric field are caused to appear by the mutual interaction arising from the oscillation of free electrons in the metallic shell layer. Such resonant peaks disappear with the reduction of the volume fraction of the core ratio f and the increase of the inter-particle distance L. It is evident that the magnitude of the E field along the θ direction decreases gradually. And the magnitude of the electric field outside the NPs is almost nine times larger than the one inside. To compare with these numerical results, simulations have also been carried out. A good agreement between them has been achieved.

Our systems involving field-induced chains of core/shell NPs offer a different way for obtaining a surface enhanced Raman scattering (SERS) substrate with the utilization of enhanced electric fields. SERS is a near-field optical phenomenon for the single-molecule detection, which relies on the intensified electric fields on a metal nanostructure when its localized surface plasmon resonance is excited by light.[34] Up to now, exploring a novel approach to fabricate an SERS substrate with strong hot spots and reproducible SERS enhancement factors is a topic of much importance. A simple strat-

egy for the formation of extraordinary large electric-field enhancements can be achieved by depositing a silver nanocube (nanosphere, nanorod) on a metal substrate.[35] For the ferromagnetic nanocomposites in our proposed soft ferrofluids, they will form an ordered chain with the applied magnetic field. Enhanced electromagnetic field effects can be generated close to the metal surface, which stem from the electromagnetic coupling between nanoparticles or from periodically ordered metal nanostructures, providing an effective SERS platform for the single-molecule detection.[17] Also, with the combination of magnetic properties and optical response, such core/shell NPs might be widely used in biomedical drug delivery, sensors, bio-imaging, and so on.[36]

References

[1] Chaudhuri R G and Paria S 2011 *Chem. Rev.* **40** 4167
[2] Li W S, Zhang J, Dong H F, Chu K, Wang S C, Liu Y and Li Y M 2013 *Chin. Phys. B* **22** 018102
[3] Cho S G, Jeon K W, Moon K W, Kim J B, Kim K H and Kim J 2011 *J. Appl. Phys.* **109** 07B533
[4] Pal S, Morales M, Mukherjee P and Srikanth H 2009 *J. Appl. Phys.* **105** 07B0504
[5] Prozorova T, Katabya G, Prozorovb R and Gedanken A 1999 *Thin Solid Films* **340** 189
[6] Lyon J L, Fleming D A, Stone M B, Schiffer P and Williams M E 2004 *Nano Lett.* **4** 719
[7] Wang L, Luo J, Fan Q, Suzuki M, Suzuki I S, Engelhard M H, Lin Y, Kim N, Wang J Q and Zhong C J 2005 *J. Phys. Chem. B* **109** 21593
[8] Wang L, Luo J, Shan S, Crew E, Yin J, Wallek, Wong S and Zhong C J 2011 *Anal. Chem.* **83** 8688
[9] Xu Z, Hou Y and Sun S 2007 *J. Am. Chem. Soc.* **129** 8698
[10] Seto T, Akinaga H, Takano F, Koga K, Orii T and Hirasawa M 2005 *J. Phys. Chem. B* **109** 13403
[11] Da'ddato S, Grillo V, Altieri S, Frabboni S, Rossi F and Valeri S 2011 *J. Phys. Chem. C* **115** 14044
[12] Crisana O, Angelakerisb M, Flevarisb N K and Filotia G 2003 *J. Opt. & Adv. Mater.* **5** 959
[13] Zhang R C, Liu L and Xu X L 2011 *Chin. Phys. B* **20** 086101
[14] Nikoobakht B and El-Sayed M A 2003 *Chem. Mater.* **15** 1957
[15] Robinson I, Tung L D, Maenosono S, Waltid C and Thanh N T K 2010 *Nanoscale* **2** 2624
[16] Shen Y, Fan D H, Fu J W and Yu G P 2011 *Acta Phys. Sin.* **60** 117302 (in Chinese)
[17] Zhou X, Fang J S, Yang D W and L X P 2012 *Chin. Phys. B* **21** 084202
[18] Patil A, Ohashi T, Buldum A and Dai L 2006 *Appl. Phys. Lett.* **89** 103103
[19] Ding X, Jia Y X and Wei E B 2012 *Chin. Phys. B* **21** 057202
[20] Wei E B, Sun L and Yu K W 2010 *Chin. Phys. B* **19** 107802
[21] Rosensweig R E 1985 *Ferrohydrodynamics* (New York: Cambridge University Press)
[22] Bai X K, Pu S L, Wang L W, Wang X, Yu G J and Ji H Z 2011 *Chin. Phys. B* **20** 107501
[23] Lam J 1986 *J. Appl. Phys.* **60** 4230
[24] Ruth D M and Thomas B J 1988 *J. Phys. D: Appl. Phys.* **21** 527
[25] Tian W J, Huang J P and Yu K W 2009 *J. Appl. Phys.* **105** 102044
[26] Cecilia N 2007 *J. Phys. Chem. C* **111** 3806
[27] Vial A and Laroche T 2008 *Appl. Phys. B* **93** 139
[28] Jornson P B and Christy R W 1972 *Phys. Rev. B* **6** 4370
[29] Fan C Z and Huang J P 2006 *Appl. Phys. Lett.* **89** 141906
[30] Boyd R W 1992 *Nonlinear Optics* (New York: Academic Press)
[31] Huang J P and Yu K W 2006 *Phys. Rep.* **431** 87
[32] Bergman D J and Stroud D 1992 *Solid State Phys.* **46** 147
[33] Chiharu M, Satoshi T, Masayuki H and Kensuke A 2010 *J. Phys.: Condens. Matter* **22** 016005
[34] Kleinman S L, Frontiera R R, Henry A, Dieringe J A and Duyne R P V 2013 *Phys. Chem. Chem. Phys.* **15** 21
[35] Rycenga M, Xia X H, Moran C H, Zhou F, Qin D, Li Z Y and Xia Y N Angew 2011 *Chem. Int. Ed. Engl.* **50** 5473
[36] Doria G, Conde J, Veigas B, Giestas L, Almeida C, Assuncao M, Rosa J and Baptista P V 2012 *Sensors* **12** 1657